Prediction of COVID-19 from Chest X-ray Images Using Multiresolution Texture Classification with Robust Local Features

Zakariya A. Oraibi
Dept. of Computer Science
College of Education for Pure Sciences, University of Basrah
Basrah, Iraq
Email: zakaria_au@uobasrah.edu.iq

Safaa Albasri
Dept. of Electrical Engineering and Computer Science
College of Engineering, University of Missouri-Columbia
Missouri, USA
Email: saaxfc@umsystem.edu

***Abstract*—The COVID-19 contagious disease that spread around the world, have a huge risk on people and already caused millions of deaths forcing a global pandemic in 2020. Diagnosing patients with this disease is very critical allowing fast care response and to isolate them from public. As the virus spread widely to millions of people, the fastest way to detect it is by analyzing radiology images. Early studies showed irregularity in the chest X-ray images of patients with high clinical belief of COVID-19 infection. Hence, these studies motivated us to investigate the use of machine learning techniques to help diagnosing COVID-19 patients from chest CT scans. In this paper, we propose to use a robust feature extraction descriptor and to apply a Random Forests classifier to predict COVID-19 disease in a dataset of 5000 images. First, 408 texture features are extracted using a powerful variation of Local Binary Patterns descriptor called Rotation Invariant Co-occurrence among Local Binary Patterns. Then, Random Forests classifier is used with 250 trees to perform the classification task. Moreover, the performance of our approach was improved by using a multiresolution scheme where features are extracted from both the original image and the subsampled image. Two metrics were used to evaluate our approach, sensitivity and specificity. We achieved 99.0% and 91.3% for both metrics, respectively. Our results are close to the state-of-the-art deep learning methods on the same dataset.**

***Index Terms*—COVID-19, Random Forests, Texture Features, X-ray Imaging.**

I. Introduction

Coronavirus (SARS-CoV-2) disease caused by severe respiratory syndrome originated in Wuhan, China and spread vastly to the rest of the globe [1]. The impact of this virus led to hundreds of thousands of fatalities and millions of infections among people globally[1]. The vast spread of the virus and the increasing number of patients resulted in focusing the attention on detecting COVID-19 cases as early as possible [2], [3]. Hence, a fast and accurate diagnosis method is required which can be achieved using chest radiography imaging like Computed Tomography (CT) or X-ray imaging. These tools are easy to conduct and considered as a routine procedure for pneumonia diagnosis. The advantage of using X-ray images is the ability to visualize indexes associated with COVID-19 [4]. These X-ray images of COVID-19 patients showed irregularities which can be diagnosed by experts [5], [6]. Hence, automatic identifications of these irregularities is important given the high rate of infected people. Machine learning techniques can solve this problem by providing tools to automatic recognition of COVID-19 patients [7].

In order to apply machine learning techniques to detect COVID-19 patients, we need a dataset with enough samples of images to be used for the training and testing purposes successfully. Since there are very few datasets available publicly of COVID-19 patients, the solutions to automatically recognize COVID-19 from X-ray images are few. One of these datasets was collected by [8] and was made publicly available for researchers. This dataset has small number of images which were collected from various academic publications. Later on, Minaee et al. [7] used the same dataset to relabel the images to only keep the images with a clear mark of COVID-19 with the help of specialized radiologist. Then, the certified COVID-19 images are combined with another subeset of images taken from another dataset which is considered the negative samples for COVID-19 detection [9]. Finally, the new dataset has around 5,000 X-ray images called COVID-Xray-5k [7] which we used in this paper.

In this paper, a machine learning framework was used to classify COVID-19 from X-ray images. The framework consists of texture feature extraction, feature classification, and a multiresolution scheme to extract more features from the input image. Texture features proved to be powerful to extract essential properties in biomedical image analysis [10]–[12]. We employed a powerful variant of the famous Local Binary Pattern (LBP) descriptor called Rotation Invariant Co-occurrence among LBP (RIC-LBP) proposed by Nosaka et. al [13]. For the classification stage, we employed the Random Forests (RF) classifier with 250 trees [14]. The motivation to use the traditional texture features and the classical clas-

[1]https://www.worldometers.info/coronavirus/

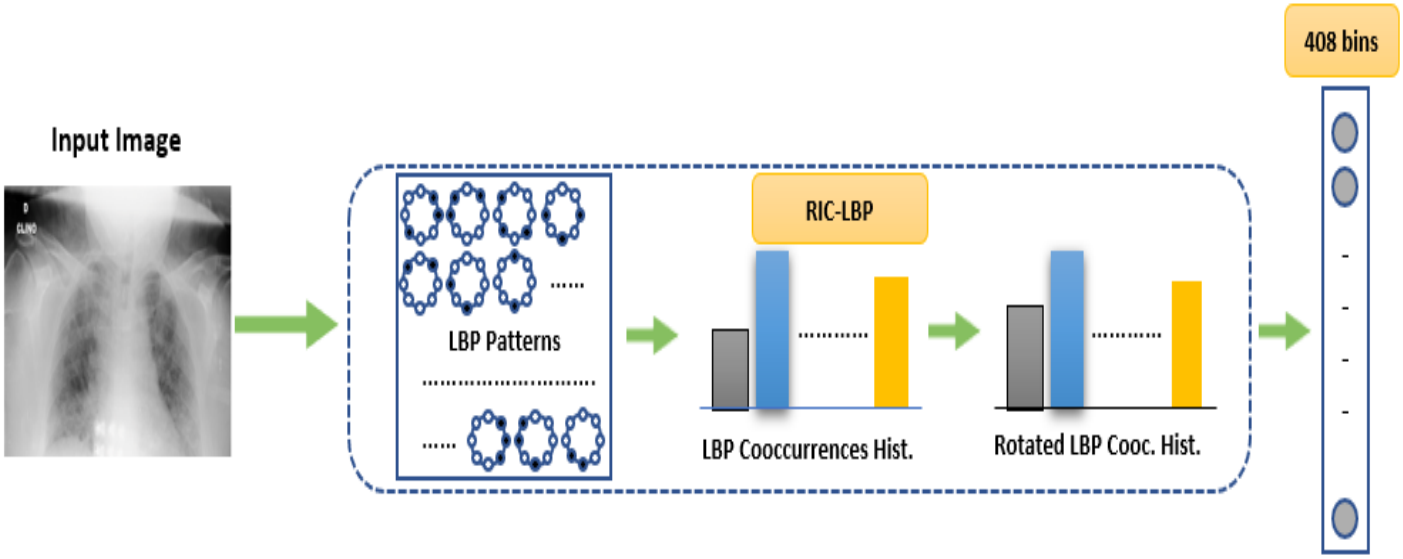

Fig. 1. Mechanism of RIC-LBP descriptor applied on chest X-ray image from the given dataset. 408 bins are calculated from the rotated LBP cooccurences histogram.

sification approach is to evaluate the performance of these methods with the already applied deep learning approaches. In addition, since there are only two classes to be predicted and the dataset is relatively small, we can show that classical machine learning algorithms are able to produce comparable results to deep learning techniques.

The rest of the paper is structured as follows. The second section details our proposed method for predicting COVID-19. Third section provides experimental results and comparison with state-of-the-art results. Finally, the fourth section concludes our paper.

II. Methodology

In this section, we detail the machine learning technique used in our paper. In general, a robust local texture feature was employed to extract the features from the input X-ray image. After that, RF classifier is applied to perform the prediction task. Furthermore, we improved the performance of our approach by using a multiresolution scheme to extract more features from the input image.

A. Texture Features

For the past two decades, local texture features using Local Binary Pattern (LBP) descriptor were used successfully to extract essential features from digital images and used these features in the prediction of many applications such as palm vein recognition [15], face recognition [16], and texture classification task [17]. After LBP was introduced, many variants of the original descriptors were proposed to improve its performance including the Rotation Invariant Co-occurrence among LBP (RIC-LBP) proposed by Nosaka et. al [13]. RIC-LBP was used to classify biomedical images and proved that the relationships between LBP patterns are important to enhance the recognition performance. In our previous work, we used RIC-LBP to extract texture features from Carbon NanoTube (CNT) forest forest classes based on varying CNT diameter and CNT density numbers [18].

The mechanism of RIC-LBP is that it exploits the relationships among the binary patterns by finding the co-occurrences patterns among the histogram features. In addition, the histogram of the descriptor is represented in the form of multiple LBP pairs where each pair will be attached with a specific label to account for rotation invariance which makes it very powerful to capture important texture features from the given image. The total number of features extracted using the RIC-LBP descriptor are 408 bins. Figure 1 illustrates the operations of RIC-LBP.

B. Multiresolution Scheme for Feature Extraction

Texture image patterns vary among different image resolutions. Capturing more patterns from multiresolution scheme showed to generate better classification performance [17]. This can be done by downsampling the original image and computing features on both the original and the subsampled images. After that, the features extracted from both images are concatenated in a late fusion mechanism and the final step is to send those features to the classification stage. Hence, this subsampling procedure helps to capture the texture patterns from the farther pixel neighbors [19].

In our previous work, we used the same multiresolution scheme to classify Human Epithelial type-2 (HE-2) images [10]. The results of concatenating features extracted from two resolutions were better than using only the features extracted from the original image. In addition, we also used this scheme to classify natural texture images, and the prediction performance has also improved [11]. Figure 2 illustrates the multiresolution scheme.

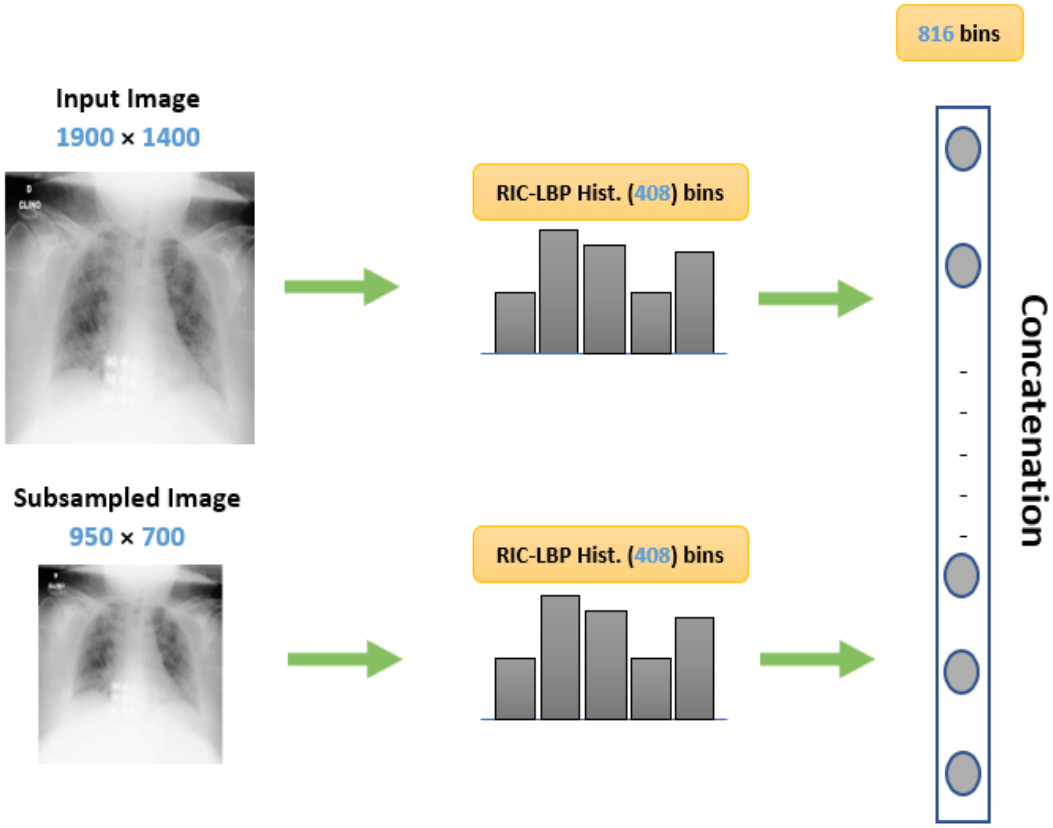

Fig. 2. Multiresolution scheme of the input image. Since chest X-ray images provided for the classification task have high resolution, when subsampling happen, shapes of the objects inside the image will be preserved. Features are extracted from both the original and the subsampled images. In total, we get 816 bins using RIC-LBP descriptor.

C. COVID Prediction using RF Classifier

RF classifier has been used for both classification and regression tasks. It is considered an ensemble learning technique that works by making many decision trees at training time and the output result is the class that is computed as the mode of the classes or mean prediction if the task is finding the regression task [14]. Therefor, RF is a divide and conquers approach.

The training algorithm for random forests uses the general technique of bagging or bootstrap aggregating. The number of trees in the model is a free parameter. In general, a few hundred to several thousand trees are used, depending on the nature and the size of the training samples. In our experiments, we used 250 trees to generate a high classification results. The advantages of using RF classifier are that it handles missing variables very well, its performance is good on large datasets, and more importantly is it takes small time to create the prediction model.

III. Experimental Results

A. COVID-Xray-5k Dataset

The dataset used in the experiments is called COVID-Xray-5k [7] which was published by Minaee et al. for the purpose of prediction of COVID-19 disease using machine learning techniques. The dataset is a combination of both X-ray and CT images. The COVID-19 images for this dataset are taken from another dataset called Covid-Chest-Dataset publishd by Joseph Cohen et al. [8]. This later dataset is updated continuously and it contains other data about patients, such as age and sex. Radiologists in [7] kept anterior-posterior images for the prediction of COVID-19 cases. The number of those anterior-posterior images were 203 X-ray images. After being examined by radiologist, only 184 images of COVID-19 were approved. As a result, we are provided with a clean labeled COVID-19 dataset.

For the Non-COVID images, there were only few number of such samples in the [8] dataset. Hence, Minaee et al. had to use images from another dataset called Chex-Pert dataset [9] collected by Irvin et al. This dataset is large with over 200,000 images of chest radiographs taken from over 65,000 patients. From this large pool of images, 2,000 Non-COVID images were selected for training and another 3,000 images for testing. This will bring the total images for the Non-COVID class to 5,000 images. Table I below shows the number of images used for both training and testing stages of each class used in our experiments. Samples of COVID and Non-COVID images are shown in Figure 3 below.

The resolution of the images provided by this dataset vary

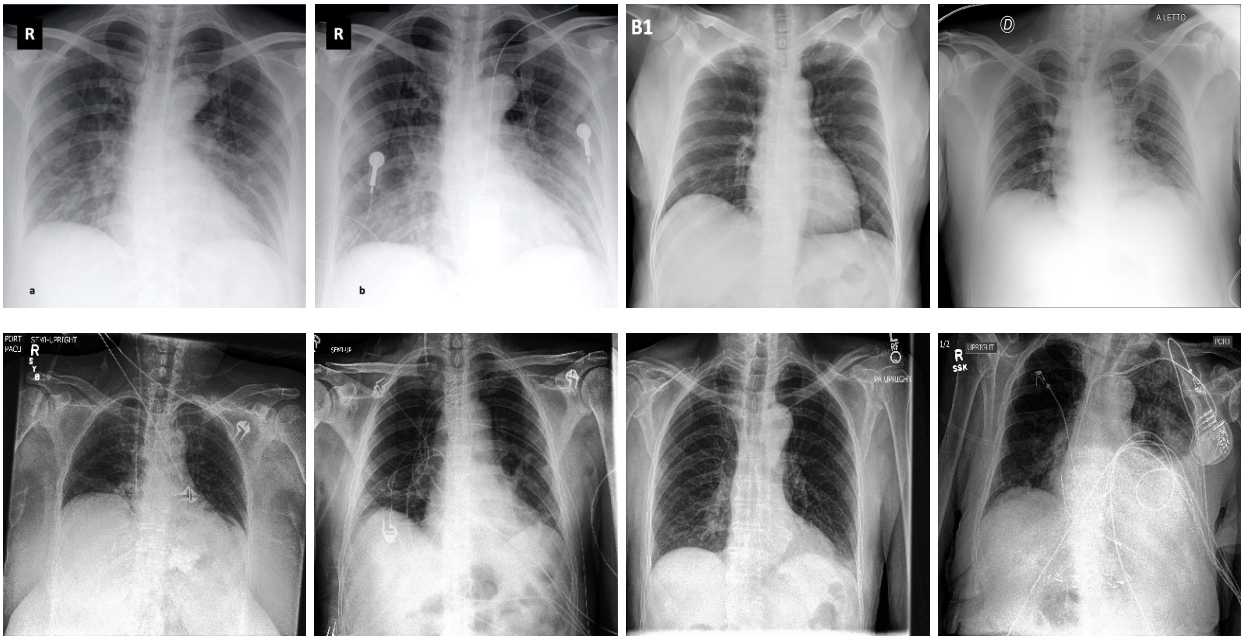

Fig. 3. Sample images from the COVID dataset. Samples of the first row are COVID-19 images. Samples of the second row are Non COVID-19 images.

TABLE I
TOTAL NUMBER OF IMAGES PER CLASS OF COVID-XRAY-5K DATASET. IT IS OBVIOUS THAT WE HAVE FEWER NUMBER OF TRAINING IMAGES COMPARED TO TESTING IMAGES.

Dataset Split	COVID-19	Non-COVID
Training Images	84	2000
Testing Images	100	3000

widely. Some images have a low resolution of only 400×400 and other images have very high resolution of 1900×1400. The reason for this variation is that images are collected from multiple sources. Since we are using local texture features, RIC-LBP descriptor will not be affected by this change. In addition, the mulltiresolution scheme, which divides the image by half, works well on these resolutions since the structure of the objects inside the image will be intact.

B. Results of Experiments

In this section, we introduce our results using our framework for feature extraction and classification. We also introduce a comparison with the state-of-the-art approaches introduced before in relation to the dataset. To evaluate the performance of the RF classifier, we used both sensitivity and specificity metrics. Since the provided dataset is imbalanced, these two metrics are proper to be used to report the classification performance. The equations to calculate both metrics are as shown below:

$$Sensitivity = \frac{TCC}{TC} \tag{1}$$

where TTC is the number of images correctly predicted as COVID-19. TC is the total number of COVID-19 images.

$$Specificity = \frac{NCC}{NC} \tag{2}$$

where NCC is the number of images correctly predicted as Non-COVID. NC is the total number of Non-COVID images.

The first experiment we conducted was extracting texture features from the original chest X-ray images and applying the RF classifier with 250 trees. In total, we get 408 bins of texture features for all training and testing images. Results for this experiment are shown in Table II below:

TABLE II
SENSITIVITY AND SPECIFICITY RATES USING RIC-LBP AND RF CLASSIFIER. 408 BINS WERE EXTRACTED FROM THE ORIGINAL IMAGE.

Model	Sensitivity	Specificity
ResNet18	**98.0**%	90.7%
ResNet50	98.0%	89.6%
SqueezeNet	98.0%	**92.9**%
Densenet-121	98.0%	75.1%
RIC-LBP (408 bins)	95.0%	89.3%

From this table, we observe that local texture features with RF classifier produced a sensitivity rate of 95% which is 3% less than the results set by state-of-the-art deep learning based methods. In addition, specificity rate achieved good scoring 89.3% outperforming Densenet-121 [22] rate and falling short to both ResNet18 [20] and ResNet50 [20]. Furthermore, it falls by more than 3% to SqueezeNet [21]. As we know, the methods used before are all deep learning approaches with transfer learning. As a result, their performance is very high.

Figure 4 shows the confusion matrix of the first experiment for the two classes in the dataset. Only 5 COVID samples were misclassified as Non-COVID samples while 320 Non-COVID samples were misclassified as COVID samples. This

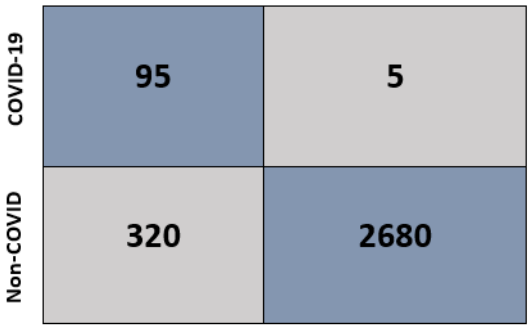

Fig. 4. Confusion matrix of RF classifier using RIC-LBP applied to the original image.

is because we need to extract more texture patterns in order to improve the classification accuracy.

The second experiment we conducted was extracting texture features from two levels of the input image. RIC-LBP was first applied to the original image resolution and a total of 408 bins texture features were extracted. Then, the original image is subsampled and the same descriptor was applied on the new image resolution to extract additional 408 bins texture features. A late fusion mechanism was applied to merge those features by concatenating the two extracted features into a single features vector. This works by adding the second set of features to the end of the first set of features which will generate 816 bins. The newly fused 816 bins texture features are then fed to the 250 trees RF classifier. Results for this experiment are shown in Table III below:

TABLE III
SENSITIVITY AND SPECIFICITY RATES USING RIC-LBP AND RF CLASSIFIER WITH MULTIRESOLUTION SCHEME APPLIED TO THE ORIGINAL IMAGE. 816 BINS WERE EXTRACTED FROM BOTH THE ORIGINAL AND THE SUBSAMPLED IMAGE.

Model	Sensitivity	Specificity
ResNet18	98.0%	90.7%
ResNet50	98.0%	89.6%
SqueezeNet	98.0%	**92.9**%
Densenet-121	98.0%	75.1%
RIC-LBP (816) bins	**99.0**%	91.3%

Both sensitivity and specificity rates were improved by using the multiresolution scheme in extracting the features. RIC-LBP with 816 bins scored 99% in sensitivity and 91.3% in specificity. We outperform all the deep learning methods by 1% in sensitivity and score comparable result to the best specificity rate generated by SqueezeNet architecture.

Figure 5 shows the confusion matrix of the second experiment for the two classes in the dataset. Hence, the multiresolution scheme resulted in only a single COVID sample to be mis-classified as Non-COVID. In addition, it reduced the number of mis-classified Non-COVID samples from 320 to 259. Thus, multiresolution approach for texture features extraction proved to generate better results on chest X-ray images using the RF classifier.

It is worthy to mention that the choice of the number of trees was made based on the experiments illustrated in Figure 6. We started with a value of 25 and performed experiments up until the value of 500 where the rates for sensitivity and specificity dropped. The graph on the left represents experiments performed using RIC-LBP with 408 bins. While the graph on the right represents experiments performed using RIC-LBP with 816 bins. The highest values for sensitivity and specificity rates for both graphs were achieved using an RF classifier with 250 trees.

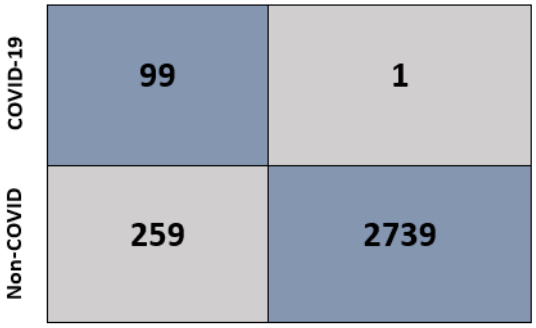

Fig. 5. Confusion matrix of RF classifier using RIC-LBP applied to the multiresolution scheme.

IV. CONCLUSIONS

This paper presents a simple classical machine learning framework to predict COVID-19 disease from X-ray images. Two stages involved in this prediction task: feature extraction and classification. For the feature extraction, we used a powerful texture features descriptor that showed high performance to classify biomedical images called RIC-LBP descriptor. For the classification task, we also used a strong classifier called Random Forests (RF) with 250 trees. The proposed framework, which includes a multiresolution scheme to enrich the extracted features from the input image, was applied on a benchmark dataset of 5,000 images. Results showed that classical machine learning approaches performed good given the small number of X-ray images provided and the fact that we are only trying to predict two classes. We scored 99.0% and 91.3% in sensitivity and specificity, respectively. We also compared our results with deep learning approaches tested previously on the same dataset and our performance using the texture feature and RF classifier is considered comparable with the previous work.

In the future, we intend to build our own deep learning architecture to classify X-ray images for this task to further improve the classification metrics. In addition, we hope in the future, a much bigger and comprehensive COVID-19 dataset becomes available so that we can produce an efficient classification approach with better classification results.

REFERENCES

[1] W. Wang, Y. Xu, R. Gao, R. Lu, K. Han, G. Wu, and W. Tan, "Detection of sars-cov-2 in different types of clinical specimens," *Jama*, vol. 323, no. 18, pp. 1843–1844, 2020.

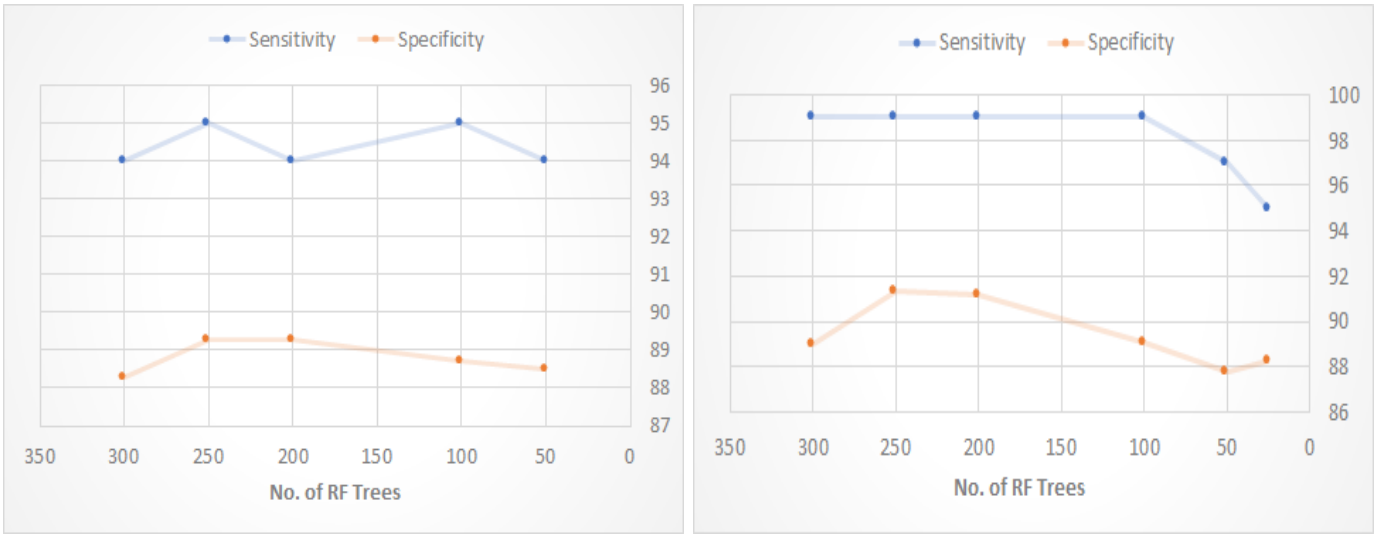

Fig. 6. Illustration of the choice of the number of trees parameter during the experiments. The graph on the left shows the classification rates using RIC-LBP with 408 bins. The graph on the right shows the classification rates using RIC-LBP with 816 bins. Our best results came from using 250 trees.

[2] C. Rothe, M. Schunk, P. Sothmann, G. Bretzel, G. Froeschl, C. Wallrauch, T. Zimmer, V. Thiel, C. Janke, W. Guggemos, *et al.*, "Transmission of 2019-ncov infection from an asymptomatic contact in germany," *New England Journal of Medicine*, vol. 382, no. 10, pp. 970–971, 2020.

[3] Q. Li, X. Guan, P. Wu, X. Wang, L. Zhou, Y. Tong, R. Ren, K. S. Leung, E. H. Lau, J. Y. Wong, *et al.*, "Early transmission dynamics in wuhan, china, of novel coronavirus–infected pneumonia," *New England Journal of Medicine*, 2020.

[4] J. P. Kanne, B. P. Little, J. H. Chung, B. M. Elicker, and L. H. Ketai, "Essentials for radiologists on covid-19: an update—radiology scientific expert panel," 2020.

[5] D. M. Hansell, A. A. Bankier, H. MacMahon, T. C. McLoud, N. L. Muller, and J. Remy, "Fleischner society: glossary of terms for thoracic imaging," *Radiology*, vol. 246, no. 3, pp. 697–722, 2008.

[6] G. D. Rubin, C. J. Ryerson, L. B. Haramati, N. Sverzellati, J. P. Kanne, S. Raoof, N. W. Schluger, A. Volpi, J.-J. Yim, I. B. Martin, *et al.*, "The role of chest imaging in patient management during the covid-19 pandemic: a multinational consensus statement from the fleischner society," *Chest*, 2020.

[7] S. Minaee, R. Kafieh, M. Sonka, S. Yazdani, and G. J. Soufi, "Deep-covid: Predicting covid-19 from chest x-ray images using deep transfer learning," *arXiv preprint arXiv:2004.09363*, 2020.

[8] J. P. Cohen, P. Morrison, L. Dao, K. Roth, T. Q. Duong, and M. Ghassemi, "Covid-19 image data collection: Prospective predictions are the future," *arXiv preprint arXiv:2006.11988*, 2020.

[9] J. Irvin, P. Rajpurkar, M. Ko, Y. Yu, S. Ciurea-Ilcus, C. Chute, H. Marklund, B. Haghgoo, R. Ball, K. Shpanskaya, *et al.*, "Chexpert: A large chest radiograph dataset with uncertainty labels and expert comparison," in *Proceedings of the AAAI Conference on Artificial Intelligence*, vol. 33, pp. 590–597, 2019.

[10] V. S. Prasath, Y. M. Kassim, Z. A. Oraibi, J.-B. Guiriec, A. Hafiane, G. Seetharaman, and K. Palaniappan, "Hep-2 cell classification and segmentation using motif texture patterns and spatial features with random forests," in *Pattern Recognition (ICPR), 2016 23rd International Conference on*, pp. 90–95, IEEE, 2016.

[11] Z. A. Oraibi, M. Irio, A. Hafiane, and K. Palaniappan, "Texture classification using multiple local descriptors," in *2017 IEEE Applied Imagery Pattern Recognition Workshop (AIPR)*, pp. 1–7, IEEE, 2017.

[12] Z. A. Oraibi, H. Yousif, A. Hafiane, G. Seetharaman, and K. Palaniappan, "Learning local and deep features for efficient cell image classification using random forests," in *2018 25th IEEE International Conference on Image Processing (ICIP)*, pp. 2446–2450, IEEE, 2018.

[13] R. Nosaka and K. Fukui, "HEp-2 cell classification using rotation invariant co-occurrence among local binary patterns," *Pattern Recognition*, vol. 47, no. 7, pp. 2428–2436, 2014.

[14] T. K. Ho, "Random decision forests," in *Proceedings of 3rd international conference on document analysis and recognition*, vol. 1, pp. 278–282, IEEE, 1995.

[15] L. Mirmohamadsadeghi and A. Drygajlo, "Palm vein recognition with local binary patterns and local derivative patterns," in *2011 International Joint Conference on Biometrics (IJCB)*, pp. 1–6, IEEE, 2011.

[16] D. Huang, C. Shan, M. Ardabilian, Y. Wang, and L. Chen, "Local binary patterns and its application to facial image analysis: a survey," *IEEE Transactions on Systems, Man, and Cybernetics, Part C (Applications and Reviews)*, vol. 41, no. 6, pp. 765–781, 2011.

[17] T. Ojala, M. Pietikainen, and T. Maenpaa, "Multiresolution gray-scale and rotation invariant texture classification with local binary patterns," *IEEE Transactions on pattern analysis and machine intelligence*, vol. 24, no. 7, pp. 971–987, 2002.

[18] T. Hajilounezhad, Z. A. Oraibi, R. Surya, F. Bunyak, M. R. Maschmann, P. Calyam, and K. Palaniappan, "Exploration of carbon nanotube forest synthesis-structure relationships using physics-based simulation and machine learning," in *IEEE Applied Imagery Pattern Recognition Workshop*, 2019.

[19] A. Hafiane, K. Palaniappan, and G. Seetharaman, "Joint adaptive median binary patterns for texture classification," *Pattern Recognition*, vol. 48, no. 8, pp. 2609–2620, 2015.

[20] K. He, X. Zhang, S. Ren, and J. Sun, "Deep residual learning for image recognition," in *Proceedings of the IEEE conference on computer vision and pattern recognition*, pp. 770–778, 2016.

[21] F. N. Iandola, S. Han, M. W. Moskewicz, K. Ashraf, W. J. Dally, and K. Keutzer, "Squeezenet: Alexnet-level accuracy with 50x fewer parameters and¡ 0.5 mb model size," *arXiv preprint arXiv:1602.07360*, 2016.

[22] G. Huang, Z. Liu, L. Van Der Maaten, and K. Q. Weinberger, "Densely connected convolutional networks," in *Proceedings of the IEEE conference on computer vision and pattern recognition*, pp. 4700–4708, 2017.